ANALYSIS OF WIMP, FIMP AND SIMP DARK MATTER PRODUCTION MECHANISMS IN THE PRIMORDIAL UNIVERSE

Mateo Escorcia Sierra

Director:

Nicolás Bernal, PhD

Codirector:

Mario Andrés Acero Ortega, PhD

Universidad del Atlántico

Faculty of Basic Sciences

Physics Programme, PEyCOS research group

Puerto Colombia, Colombia

2023

Contents

Chapter 1

Abstract

In this study we examine the mechanisms of dark matter production in the primordial or early universe, focusing on the WIMP, FIMP and SIMP approaches. Fundamental differences were found between these mechanisms, where WIMP and SIMP followed the thermal equilibrium until their freeze-out, while FIMP is never in this equilibrium and was highly sensitive to the initial conditions of the analyzed equations. Furthermore, it was identified that, for WIMP and SIMP, the relic mass and the effective cross-section were inversely proportional to the final number density, while for FIMP they were directly proportional. On the other hand, approximate solutions were developed for the WIMP and SIMP mechanism that were significantly close to the numerical results. All cases were compared with observational data, thus obtaining congruent results. These findings contribute to a deeper understanding of dark matter production and its relevance in high energy physics.

Chapter 2

Introduction

The nature and origin of dark matter is one of the greatest enigmas in physics today. What generates this intrigue is precisely that it is very difficult to study and observe, since what we define as dark matter is a body that does not present any type of electromagnetic interaction, only manifesting itself through gravitational interactions with baryonic matter, or depending on the model being studied, with other dark matter bodies. [1].

The first to propose the concept of dark matter was Fritz Zwicky in 1933 [2]. Who while studying the rotation speed of different galaxy clusters, he found that the Coma cluster rotated at a higher speed than his calculations predicted. Zwicky proposed the concept of dark matter as an answer. His explanation for this behavior was that the cluster possessed more mass than could be detected .This caused the total mass of the cluster to increase and only in this way could the system reach the velocities that were measured. Other scientists were skeptical of his theory, but as time went on similar results were found in other clusters. [3].

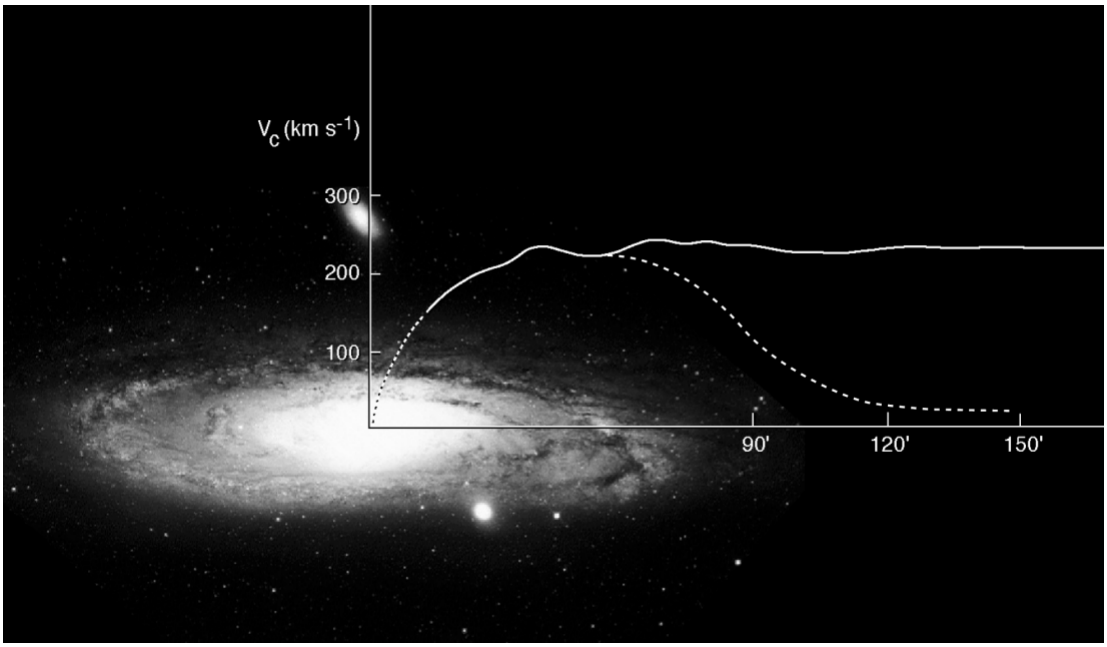

Figure 2.1: Image of the Andromeda galaxy and its rotation curves. Circular velocity of the gas cloud and stars orbiting the galaxy center (km/s) vs distance to the galaxy center (arcmin). The solid line represents the observed data and the dashed line shows the rotation curves calculated without accounting for the effect of dark matter. Image created by M. Roberts. [4]

The modern stage of dark matter research began in the 1970s, caused by the need to explain the gaseous kinematics of galaxies, where it was found that the velocity of galactic gas in these systems did not decrease once the limits of the stellar disk were passed, which made the existence of some phenomenon that caused these high velocities in celestial systems unquestionable.

It is important to mention and discuss now the cosmic microwave background (CMB) *Cosmic Microwave Background*, which plays a fundamental role in particle physics by providing a crucial window to understand the events that happened during the early universe. This remnant of Big Bang radiation, which is found throughout the observable universe, has made it possible to study the primordial fluctuations that gave rise to the cosmic structures we observe today. By analyzing the CMB, it has been possible to obtain valuable information about the composition and evolution of the early universe, as well as to confirm important

predictions of the Big Bang theory. In relation to dark matter, the CMB plays a crucial role in providing clues about the distribution and nature of dark matter in the universe. While dark matter itself does not interact directly with CMB radiation, its presence is evident through its gravitational effects on the formation of large-scale structures in the universe. The anisotropies observed in the CMB reflect primordial density fluctuations, which are composed of both baryonic matter and dark matter, thus providing valuable information for understanding the distribution of matter in the early universe.

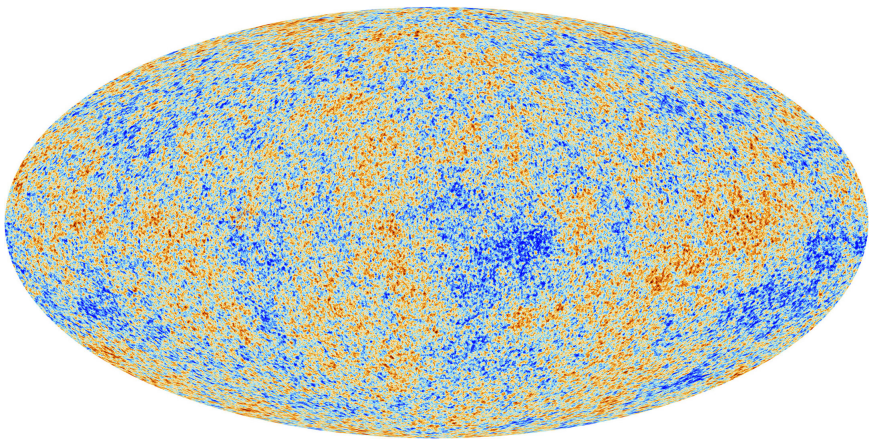

Figure 2.2: Image of the cosmic microwave background captured by Planck telescope [5]

Figure (2.2) shows the typical seen CMB image, which reveals a uniform distribution of microwave radiation, with small variations indicating anisotropies in the radiation. These variations are crucial for understanding the evolution and composition of the early universe. By studying these variations, scientists can map primordial density fluctuations and better understand the formation of cosmic structures over cosmic time, providing essential information about the nature and origin of the universe as we know it. In addition, these data can be used to plot the angular power spectrum of the CMB, and thus find the energy density composition of the universe.

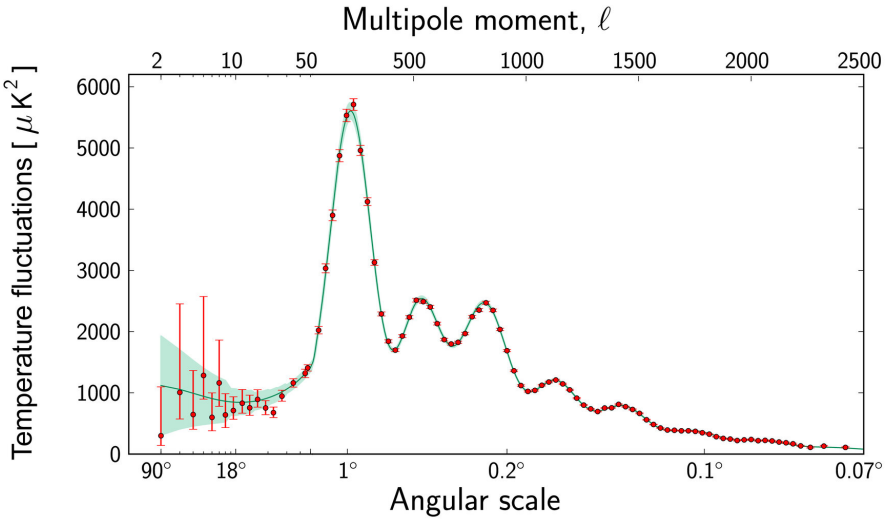

Figure 2.3: Plot of the temperature fluctuations in the CMB detected by the Planck telescope at different angular scales, starting from ninety degrees on the left side of the plot to zero on the right side. [6]

In Figure (2.3), The plot of the CMB power spectrum, obtained from precise observations by the Planck satellite, is crucial for understanding the fluctuations in cosmic microwave radiation as a function of its angular scale. This representation visualizes the anisotropies in the CMB and provides detailed information about density variations in the early universe. From this power spectrum, a statistical analysis can be performed to determine the density composition of the universe. Using these observations and calculations, the energy density of the universe was found to be composed of approximately 70 percent dark energy, 26 percent dark matter and only 4 percent ordinary matter [5], which is composed of particles called baryons and is referred to as baryonic matter. These data suggest that the current energy density takes values approximating to [5]

$$\rho_0 \approx \frac{3H_0^2}{8\pi G_N} \approx 10^{-29}\ \mathrm{g/cm^3} \approx 10^{-26}\mathrm{kg/m^3}, \tag{2.1}$$

where H_0 is the current Hubble parameter and G_N is the gravitational constant, this would correspond to an average density of 10 protons per cubic meter. [7].

Fortunately, dark matter can also be studied from the point of view of particle physics. There are many possible candidates for dark matter, each with its own advantages and disadvantages, but all of them have to satisfy conditions and characteristics that have been observed in dark matter. For a particle to be considered a viable option, it is expected to be electrically neutral, without color charge, to interact weakly with baryonic matter, and to be stable or have a lifetime greater than the age of the universe, which has been calculated to be approximately 13.7 billion years old. [1]. In addition, it is necessary that the model is able to generate the amount of dark matter that has been measured so far, which is expressed as [8]

$$\Omega_{DM} \equiv \frac{\rho_{DM,0}}{\rho_0} \approx 0.26, \tag{2.2}$$

where $\rho_{DM,0}$ is the presently measured dark matter density, and can be expressed as

$$\rho_{DM,0} \approx 10^{10} \frac{M_\odot}{\text{Mpc}^3} \approx 10^{-6} \ \frac{\text{GeV}}{\text{cm}^3}, \tag{2.3}$$

And $M_\odot$ corresponds to the mass of the Sun. If all these criteria are met, it has a potential prospect to be the particle that makes up dark matter.

In this study, we conducted an analysis of some of the mechanisms of dark matter production in the early universe, where the particles generated meet the criteria stated above. Since this subject is still heavily researched, there are many different mechanisms that try to explain such production. This study concentrates on three of these mechanisms. The first, and the most widely known, is The Weakly Interacting Massive Particles or WIMP mechanism, which is studied by applying the Boltzmann equations to examine the behavior of WIMP relics in the thermal bath during the early moments of the universe. This analysis is conducted by finding an approximate analytical solution and a numerical solution using Python programming. Once the results are obtained, the calculations are adapted to characterize the Feebly Interacting Massive Particles or FIMP and Strongly Interacting Massive Particles or SIMP

mechanisms. The particles that generate these three production mechanisms stand out for being beyond the standard model. It is important to mention that there is no particle within the standard model that has the necessary characteristics mentioned above. This necessitates searching beyond what has been defined in the standard model in the quest for candidates for dark matter particles, thereby creating an immense number of possible explanations for the true nature of dark matter.

The specific objectives of the study included initially understanding the astrophysical and cosmological motivations behind the investigation of dark matter. Subsequently, the thermodynamics of the primordial universe was studied, followed by an analysis and comparison of the three mentioned production methods (WIMPs, FIMPs, and SIMPs). Finally, an analytical and numerical approximation of the Boltzmann equations for the mechanisms were found to compare their thermodynamic evolutions with the observed dark matter number density.

This study is divided into four sections. It starts with a presentation of the theoretical foundations necessary to understand the premise of this work. These foundations are detailed in the Theoretical Framework section, where the three methods of dark matter production that will be worked on are explained, followed by the introduction of the Boltzmann equations. Their utilities and functions are described, and then applied to each of the mechanisms under study. The following section is called Methodology, which presents the form and methods employed to achieve the results of this work. Calculations were carried out, and the procedures to find an approximate analytical solution to the Boltzmann equations for the WIMP production mechanism are shown, followed by finding the solution to these same equations, but this time numerically using computational methods and Python programming. Once the results for the WIMP model are obtained, the problem formulation is modified to adapt to the characteristics of the SIMP and FIMP production methods. In the Analysis and Results Discussion section, the analytical results acquired in each model are explained, highlighting the differences between them. Subsequently, a graphical comparison of the numerical results

acquired for each production method is conducted.

The document concludes with the final section named Conclusions, where the key differences found between the three production mechanisms are expressed along with important characteristics of each, primarily the relationship found between the numerical density, the effective section, and the mass of the dark matter particle.

Chapter 3

Theoretical Framework

3.1 WIMPs

The Weakly Interacting Massive Particles (WIMP) paradigm is one of the predominant production mechanisms in the search for dark matter. Its popularity stems from the existence of several theories where these particles already appeared and would play a significant role [9]. They would have a description that perfectly fits the requirements of the dark matter particle, which are to be non-relativistic at the time of their production, neutral, and weakly interacting with baryonic matter. Like the other production mechanisms discussed in this document, the WIMP mechanism operates with particles beyond the standard model. The main problem with WIMPs is that, despite experiments being conducted at the Large Hadron Collider (LHC) to produce particles of this type [10], no particle of this nature has been observed within the expected energy ranges.

In addition to these experiments, numerous projects are also underway to find evidence of WIMPs, both using direct detection and indirect detection methods. Direct detection involves the detection of particles by observing their interaction with the detector. In this case, WIMP particles pass through the detector, and occasionally interact with the material inside the system, generating a measurable signal for the detector [11]. An example of direct detec-

tion experiments for WIMP particles is the experiments conducted by the LUX-ZEPELIN detector. This is one of the largest dark matter direct detection experiments in the world. It is designed to detect WIMPs through their interaction with ultrapure xenon nuclei in an underground detector at the Sanford Underground Research Facility in the United States [12].

On the other hand, there is also a large number of experiments attempting to detect traces of WIMPs using indirect detection methods. This type of detection is characterized by observing the effects or consequences of the presence of certain particles or phenomena, rather than directly detecting the particles themselves. For WIMPs, researchers typically search for the products of annihilation or decay of these particles. This involves searching for radiation signals, such as gamma rays, cosmic rays, neutrinos, or other secondary particles that may arise from the interaction of dark matter. An example of such experiments is those conducted by the Fermi Large Area Telescope (Fermi-LAT). This is a space observatory that detects high-energy gamma rays. Although its main objective is to study astrophysical sources of gamma rays, it can also provide indirect evidence of the presence of WIMPs through the observation of possible signals of dark matter annihilation in regions of space where a high concentration of dark matter is expected [13].

An important characteristic of the WIMP production mechanism is its behavior during chemical decoupling, which is the moment in the early universe when particles of different types fall out of chemical equilibrium. In this state, the production and annihilation reactions of different particles occurred with the same interaction rate [8]. During this period, the annihilation rate of dark matter Γ competes with the expansion of the universe described by the Hubble parameter H. The process begins with $\Gamma >> H$, where annihilation is very efficient due to high temperatures and the proximity of particles. However, as the universe expands, Γ decreases until $\Gamma \approx H$. At this point, annihilation ceases to be efficient, and it is said that dark matter undergoes "Freeze-out" [7]. Particles remaining after a freeze-out are termed hot relics if they are relativistic, or cold relics if they are non-relativistic. Their abundance remains constant from this point onwards. The interaction rate Γ can be described in general for processes in thermal decoupling by considering an effective cross-section σ, number

density n, and relative velocity v:

$$\Gamma = n\sigma v, \tag{3.1}$$

where we can express the number density as

$$n_{EQ}(T) = \frac{gm^2T}{2\pi^2}K_2\left(\frac{m}{T}\right), \tag{3.2}$$

This is its general form, where $K_2(x)$ is the second kind Bessel function, and g is the number of internal degrees of freedom of the system. It is also common to see this equation being approximated for relativistic and non-relativistic limits [14].

$$n_{rel} \propto T^3 \quad \text{for } m << T, \tag{3.3}$$

$$n_{no-rel} \propto (mT)^{3/2}e^{-m/T} \quad \text{for } m >> T, \tag{3.4}$$

And we can observe how the subscripts indicate that, depending on the relationship between the mass of the particles and the temperature of the thermal bath, they tend to be mostly relativistic or non-relativistic [8]. It has also been predicted that the mass of the cold relics in question would be

$$m_{DM} \approx \alpha_{ann}(T_{eq}m_{pl})^{1/2} \approx 1\ \text{TeV}, \tag{3.5}$$

where α_{ann} is the coupling constant of the effective annihilation cross-section of dark matter $2 \to 2$, $T_{\text{eq}} \approx 0.8$ eV is the radiation-matter equality temperature, and $m_{\text{pl}} = 1.22 \times 10^{19}$ GeV is the Planck mass.

3.2 FIMPs

It was stated that for the previous mechanism, relics began with high abundance, which decreases through an annihilation process until $\Gamma \approx$ H, where freeze-out occurs. This is where

WIMPs differ from Feebly Interacting Massive Particles (FIMP), also known as Freeze-In Massive Particles [15]. Instead of reaching the freeze-out point where it becomes constant after a large number of annihilations, the FIMP mechanism starts with low relic abundance, and these relics are produced during thermal decoupling until reaching the constant abundance we have today.

We can designate the FIMP relic as X, and assume that at temperatures much higher than the electroweak scale, this particle is very weakly coupled with the thermal bath through a renormalizable interaction. This implies that the equations describing how the particles interact can be adjusted and mathematically corrected, so that the calculations do not lead to infinite or physically meaningless results. The interaction vertex may involve more than one particle from the thermal bath, where we designate the mass of the heavier particle as m, which is considered to have values close to the electroweak scale. For a Yukawa interaction or a fourth-order interaction, where the relative masses of the particles affect the strength and rate of interaction, we have a dimensionless coupling called λ, and for a scalar three-vertex interaction, this coupling would be λm, where $\lambda << 1$ [15].

Due to the weak interaction between dark matter and standard matter in the freeze-in model, the search for FIMP particles through direct detection or experiments at the LHC becomes very difficult to perform. Nevertheless, the FIMP mechanism has started to gain momentum due to the unsatisfactory results of experiments and projects attempting to detect WIMP particles. There are several candidates that could satisfy a freeze-in mechanism, but one of the most studied is sterile neutrinos. They are considered an extension of the standard model, which could solve the mystery of the current abundance of dark matter in addition to contributing to neutrino research, leading to a mechanism that would generate Majorana mass for standard model neutrinos.

As we saw earlier, the WIMP and FIMP mechanisms differ in various ways, but they also have their similarities, such as the current abundance of dark matter. This phenomenon can

be explained with both mechanisms, even though the abundance starts with very different values in the WIMP and FIMP mechanisms [16].

3.3 SIMPs

As mentioned when introducing the WIMP production method, this model is based on the assumption that dark matter is a cold relic with standard $2 \rightarrow 2$ annihilation, but the system could also function with other mechanisms, as proposed by the SIMP production method, where dark matter reaches freeze-out using a $3 \rightarrow 2$ annihilation process, where three dark matter particles collide and two are produced [17]. For this case, the mass scale would change and result in

$$m_{DM} \sim \alpha_{ann}(T_{eq}^2 m_{pl})^{1/3} \sim 100\,\mathrm{MeV}, \tag{3.6}$$

This points to a method where dark matter interacts strongly with itself and would possess a mass scale slightly below the GeV, hence the name of the model "Strongly Interacting Massive Particles" or SIMP. The SIMP method also applies to $4 \rightarrow 2$ annihilation mechanisms when the $3 \rightarrow 2$ reaction is prohibited. The estimated mass previously mentioned for SIMPs can be demonstrated by solving the Boltzmann equations explicitly, but for that, it is necessary to express some variables in measurable quantities, such as the number density.

$$n_{DM} = \frac{\xi m_P \eta s}{m_{DM}} = \frac{c T_{eq} s}{m_{DM}}, \tag{3.7}$$

where $\xi = \rho_{\mathrm{DM}}/\rho_b \approx 5.4$, [5], $m_p = 0.938$ GeV is the mass of a proton, s is the entropy density of the universe, η is the baryon density to entropy density ratio, and $T_{\mathrm{eq}} \approx 0.8$ eV is the radiation-matter equality temperature.

3.4 Boltzmann Equations

In the early universe, many particles, relics, or species can collide and create other species. To analyze these processes, we can employ techniques from statistical mechanics and describe these relics using a phase space density $f(\mathbf{x}, \mathbf{p}, t)$, which is related to the number density by the equation

$$n(t) = \frac{g}{(2\pi)^3} \int d^3p f(\vec{p}, t), \tag{3.8}$$

where g is the number of internal degrees of freedom of the particle [18]. One can note how the number density depends on t but not on $\mathbf{x}$; this is because in the early universe, during the thermal bath, the universe was highly homogeneous, so the position does not affect the relic density. We can then analyze the evolution of the number density using the Boltzmann equation, which, using operators, is represented as

$$\hat{L}[f] = \hat{C}[f], \tag{3.9}$$

where $\hat{L}$ is the Liouville operator and $\hat{C}$ is the collision operator. The covariant generalization of the Liouville operator in general relativity is expressed as

$$\hat{L} = p^\alpha \frac{\partial}{\partial x^\alpha} - \Gamma^\alpha_{\beta\gamma} p^\beta p^\gamma \frac{\partial}{\partial p^\alpha}, \tag{3.10}$$

where $\Gamma^\alpha_{\beta\gamma}$ is the Christoffel symbol. If we then use the Friedman-Robertson-Walker (FRW) metric

$$ds^2 = dt^2 - R^2(t)[dr^2 + r^2 d\theta^2 + r^2 \sin^2\theta d\phi^2], \tag{3.11}$$

where R is the scale factor, which is explicitly time-dependent, and (r, θ, ϕ) are the spherical coordinates. If we additionally assume that the dependence of the partition function f on momentum is isotropic, this implies that $f = f[E, t]$, and the Liouville operator becomes

$$\hat{L}[f(E,t)] = E\frac{\partial f}{\partial t} - H|p|^2\frac{\partial f}{\partial E}. \tag{3.12}$$

Using the definition of number density and considering it as a function of the phase space density, it is expressed as

$$n(t) = \frac{g}{(2\pi)^3}\int f(E,t)d^3p, \tag{3.13}$$

With this, the Boltzmann equation can be written as:

$$\frac{dn}{dt} + 3Hn = \frac{g}{(2\pi)^3}\int \frac{C[f]}{E}d^3p, \tag{3.14}$$

where g is the number of internal degrees of freedom of the system, and H is the Hubble parameter. More detailed information on the procedure for deriving Equation (3.12) to Equation (3.14) can be found in Appendix A. When considering interactions of particles in the form $X + a + b... \longleftrightarrow i + j + ...$, the collision operator is given by [14].

$$\begin{aligned}\frac{g}{(2\pi)^3}\int \frac{C[f]}{E}d^3p = -\int & d\Pi_\psi d\Pi_a d\Pi_b ... d\Pi_i d\Pi_j ... \\ & \times (2\pi)^4\delta^4(p_\psi + p_a + p_b ... - p_i + p_j ...) \\ & \times [(|M|^2_{\psi+a+b...\rightarrow i+j...} f_a f_b ... f_\psi(1 \pm f_i)(1 \pm f_j)...) \\ & - (|M|^2_{i+j+...\rightarrow\psi+a+b...} f_i f_j ...(1 \pm f_a)(1 \pm f_b)...(1 \pm f_\psi))],\end{aligned} \tag{3.15}$$

where initially, the phase space integration factors are used, which are described as

$$d\Pi = g\frac{1}{(2\pi)^3}\frac{d^3p}{2E}, \tag{3.16}$$

then the delta function $\delta^4(p_\psi + p_a + p_b ... - p_i + p_j ...)$ is considered, which defines the requirements of the collision operator overall indicating the conservation of momentum and energy. Next, the interaction matrix $|M|^2$ is added, which we assume to be reversible, meaning that it has the ability to determine the initial state of a system based on its final state. The

factors f_i are the phase space density factors of the particles of type i respectively. When expressing the factors $(1 \pm f_i)$ to consider Pauli exclusion in the case of the plus sign and Bose enhancement in the case of the minus sign. Now, it is more convenient to consider the problems that will be analyzed on a large scale, so a change of variables is made to work in a comoving frame, resulting in $Y = n/s$, where s is the entropy density of the universe and has the form

$$s = \frac{2\pi^2}{45} g_{*s} T^3, \tag{3.17}$$

where g_{*s} represents the effective number of relativistic degrees of freedom contributing to the entropy of the universe. This results in the derivative of s with respect to time expressed as

$$\dot{s} = -3sH, \tag{3.18}$$

where H is also

$$H = 1.66 g_*^{1/2} \frac{T^2}{m_{pl}}, \tag{3.19}$$

where g represents the effective number of relativistic degrees of freedom contributing to the energy density of the universe. At high energies, $g_{=} g_{*s} \approx 100$ can be assumed because we are working with very high temperatures. This can be clearly seen in Figure (3.1).

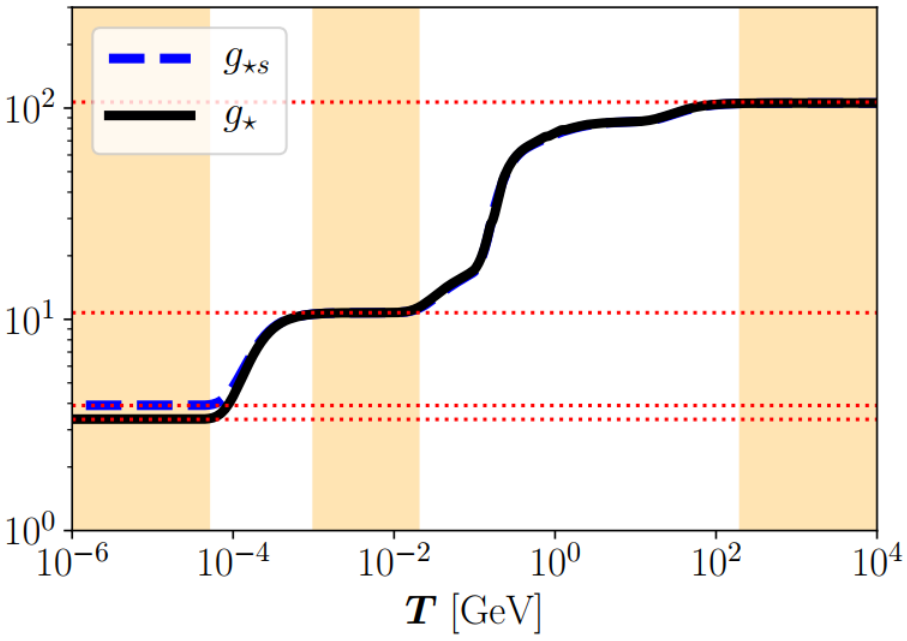

Figure 3.1: Evolution of g_* and g_{*s} as a function of temperature. Image provided by [16].

With this in mind we get to

$$\dot{Y} = \frac{\dot{n} + 3Hn}{s}, \tag{3.20}$$

It is important to note that the collision term will be expressed as a function of temperature rather than time, so another change of variable is introduced in the form $x = m/T$ where m represents the particle mass, and T the temperature. This new variable also represents time because of how the universe's temperature gradually decreases due to its expansion. Finally, combining equations (3.18), (3.19), and (**??**), we can rewrite the Boltzmann equation with more useful variables:

$$\begin{aligned} \frac{dY}{dx} = &- \frac{x}{H(m)s} - \int d\Pi_\psi d\Pi_a d\Pi_b ... d\Pi_i d\Pi_j ... \\ &\times |M|^2 (2\pi)^4 \delta^4 (p_\psi + p_a + p_b ... - p_i + p_j ... \\ &\times [f_a f_b ... f_\psi - f_i f_j ...]. \end{aligned} \tag{3.21}$$

For the analysis of the Freeze-out mechanism in the WIMP model, where a 2→2 annihilation interaction is considered [14], equations (3.14) and (**??**) are used. In this analysis, the annihilation and creation of two particles are considered to solve the collision operator, resulting in

$$\frac{dn_\psi}{dt} + 3Hn_\psi = -\langle\sigma_{\psi\bar{\psi}\to X\bar{X}}|v|\rangle\,[n_\psi^2 - (n_\psi^{EQ})^2], \tag{3.22}$$

where ψ represents the WIMP relics and X represents the particles that can generate this annihilation. Therefore, n_ψ is the number density of the relics, n_ψ^{EQ} is the equilibrium number density, and $\langle\sigma|v|\rangle$ is the cross-section. When considering the Freeze-out mechanism but with a $3 \to 2$ annihilation interaction, as described by the SIMP model, we arrive at the Boltzmann equation

$$\frac{dn_\psi}{dt} + 3Hn_\psi = -[n_\psi^3 - n_\psi^2 n_\psi^{EQ}]\,\langle\sigma v^2\rangle_{3\to 2}\,. \tag{3.23}$$

Finally, when working with the Freeze-in method as done in the FIMP model, the same equation as the WIMP mechanism is followed. However, due to its very low cross-section values, the equation is approximated to the form

$$\frac{dn_\psi}{dt} + 3Hn_\psi = \langle\sigma_{\psi\bar{\psi}\to X\bar{X}}|v|\rangle\,(n_\psi^{EQ})^2. \tag{3.24}$$

These three equations (3.22), (3.23), and (3.24) will be the ones solved during the thesis work, both analytically and numerically.

Chapter 4

Methodology

4.1 Analitical process for WIMP model

The first thing to remember about the WIMP model is that it reaches its current number density through the Freeze-out method and follows a 2→2 interaction process, meaning that in this interaction, two dark matter particles annihilate to produce two particles of the standard model, which could be of any nature but no specific ones are considered to simplify the problem. To perform this analysis, we assume that the dark matter particles are stable, allowing us to observe the current number density. It is assumed that the WIMP relics interact in the manner explained above, which can be expressed as

$$\psi\bar{\psi} \rightarrow X\bar{X}, \tag{4.1}$$

where ψ represents the dark matter particle and $\bar{\psi}$ its corresponding antiparticle, and the particles X and $\bar{X}$ represent the particles in which the relics can annihilate [14]. For this interaction to occur, energy conservation must be upheld as

$$E_{\psi} + E_{\bar{\psi}} = E_X + E_{\bar{X}}. \tag{4.2}$$

Once these characteristics of the mechanism are established, the calculation of the dark

matter relic density using equation (3.21) can begin. But before applying it to the system, certain properties are considered and assumed to simplify the equation. Initially, it is assumed that the particles X and $\bar{X}$ are in thermal equilibrium so that they follow the Maxwell-Boltzmann distribution, which is possible since relativistic particles are being worked with. Then it is considered that the chemical potential for these particles is zero because the external interactions they undergo will be much greater than those analyzed with the dark matter particles, so we consider that the particles are in chemical equilibrium. With these considerations, the distribution functions of these particles can be defined as

$$f_X = e^{-E_X/T}, \tag{4.3}$$

$$f_{\bar{X}} = e^{-E_{\bar{X}}/T}. \tag{4.4}$$

Now, recalling the conservation of energy described in equation (4.2), we can arrive at

$$f_X f_{\bar{X}} = f_\psi^{EQ} f_{\bar{\psi}}^{EQ}, \tag{4.5}$$

where the superscripts EQ represent particles in thermal equilibrium. Individually, we can express these equations as

$$f_X f_{\bar{X}} = e^{-(E_X + E_{\bar{X}})/T}, \tag{4.6}$$

$$f_\psi f_{\bar{\psi}} = e^{-(E_\psi + E_{\bar{\psi}})/T}. \tag{4.7}$$

If we return to equation (3.21), we observe that in this case it would be $[f_\psi f_{\bar{\psi}} - f_X f_{\bar{X}}]$, but through equation (4.5) it can be rewritten solely in terms of the dark matter particles.

$$[f_\psi f_{\bar{\psi}} - f_\psi^{EQ} f_{\bar{\psi}}^{EQ}]. \tag{4.8}$$

With these considerations, the other terms in (3.21) are replaced, yielding

$$\begin{aligned}\frac{dY}{dx} =& -\frac{x}{H(m)s} - \int d\Pi_{\psi} d\Pi_{\bar{\psi}} d\Pi_X d\Pi_{\bar{X}} \\ & \times |M|^2 (2\pi)^4 \delta^4(p_{\psi} + p_{\bar{\psi}} - p_X - p_{\bar{X}}) \\ & \times [f_{\psi} f_{\bar{\psi}} - f_{\psi}^{EQ} f_{\bar{\psi}}^{EQ}],\end{aligned} \tag{4.9}$$

Which can also be written as

$$\frac{dY}{dx} = \frac{-x \langle \sigma |v| \rangle s}{H(m)} (Y^2 - Y_{EQ}^2), \tag{4.10}$$

where $H(m) = 1.66 g_*^{1/2} \frac{m^2}{x^2 m_{pl}}$ and $Y = n_{\psi}/s$ as previously proposed, represents the number of relics ψ per comoving volume unit. Consequently, $Y_{EQ} = n_{\psi}^{EQ}/s$ is the number of relics ψ in equilibrium per comoving volume unit, which for cold relics has a general form given by [14]

$$Y_{EQ}(x) = \frac{45 x^2}{4\pi^4} \frac{g}{g_{*s}} K_2(x), \tag{4.11}$$

where $K_2(x)$ is the second kind Bessel function. It is common in literature to see this equation approximated for non-relativistic limits as

$$\begin{aligned}Y_{EQ} &= \frac{45}{2\pi^4} \left(\frac{\pi}{8}\right)^{1/2} \frac{g}{g_{*s}} x^{3/2} e^{-x} \\ &= 0.145 \frac{g}{g_{*s}} x^{3/2} e^{-x}.\end{aligned} \tag{4.12}$$

It is important to emphasize that equation (4.12) is only valid for non-relativistic values, so it can be used to analyze the thermodynamic evolution in the ranges of $x > 3$, since below this range relativistic physics begins to be involved. For the case of the WIMP and SIMP mechanisms, it can work perfectly, but when working with the FIMP mechanism, it is necessary to use the general form (4.11). In figure (4.1), it can be clearly seen how in the range of $x < 3$, the non-relativistic equation for Y_{EQ} deviates from the general one.

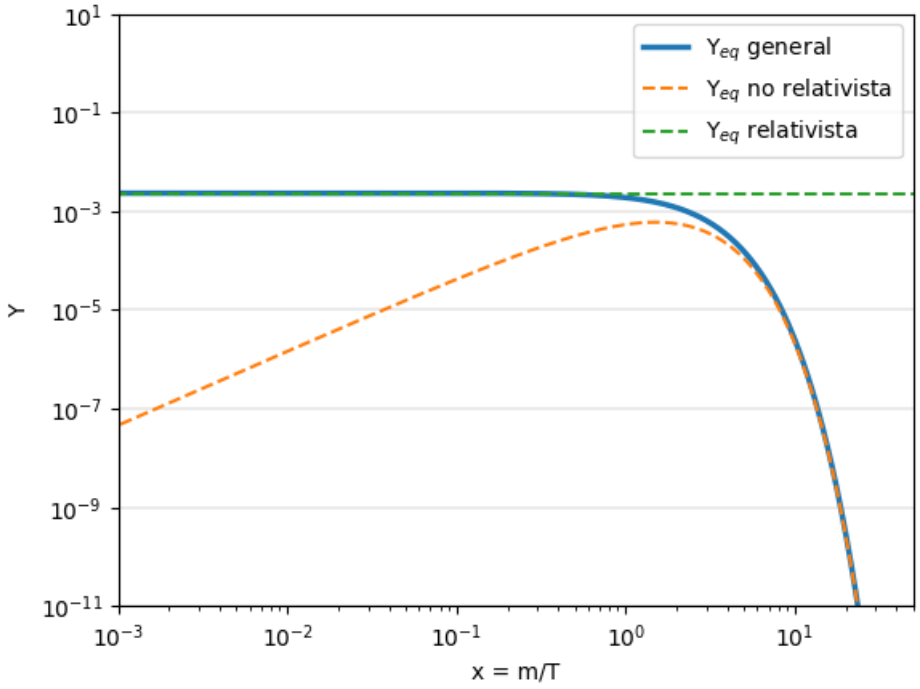

Figure 4.1: Comparison of Y_{EQ} in its general form (blue line), its non-relativistic form (orange line), and its relativistic form (green line). The vertical axis represents the numerical density Y, and the horizontal axis represents the particle mass m divided by the temperature of the universe T. Both Y and $x = m/T$ are dimensionless.

Only the definition of the annihilation cross section in equation (4.10) remains to be done; this is taken as

$$\begin{aligned}\langle \sigma v \rangle =& (n^{EQ})^{-2} \int d\Pi_{\psi} d\Pi_{\bar{\psi}} d\Pi_{X} d\Pi_{\bar{X}} |M|^2 (2\pi)^4 \\ & \times \delta^4(p_{\psi} + p_{\bar{\psi}} - p_X - p_{\bar{X}}) \\ & \times e^{-E_{\psi}/T} e^{-E_{\bar{\psi}}/T},\end{aligned} \tag{4.13}$$

The annihilation cross section plays a significant role in the analysis being conducted as it is one of the parameters that will be varied to compare the obtained results with the observed relic density today. It can also be noted that it is simply another way to formulate equation (3.22), where we consider the comoving frame of reference and the system's dependence on the temperature of the universe. Unfortunately, there is no exact solution to this Boltzmann equation, but by considering specific cases, an approximation with a good level of accuracy

can be achieved. To begin with, it should be remembered that we are analyzing the early universe where the difference between Y and Y_{EQ} must have been very low. Due to this, it is possible to focus the study on this difference, expressed as

$$\Delta = Y - Y_{EQ}, \tag{4.14}$$

and its derivative with respect to x would be

$$\frac{d\Delta}{dx} = \frac{dY}{dx} - \frac{dY_{EQ}}{dx}. \tag{4.15}$$

now we want to arrive at a form of equation (4.10) in terms of Δ and Y_{EQ}, for this, we multiply the quadratic factor that is in parentheses

$$\frac{dY}{dx} = -\lambda x^{-2}(Y^2 - Y_{EQ}^2) = -\lambda x^{-2}(Y - Y_{EQ})(Y + Y_{EQ}), \tag{4.16}$$

Where to simplify some of the calculations we call

$$\lambda = \frac{x \langle \sigma v \rangle s}{H(m)}. \tag{4.17}$$

we continue by replacing and considering equation (4.14) in equation (4.16), remembering that by rearranging we can also get $(Y + Y_{EQ}) = \Delta + 2Y_{EQ}$

$$\frac{dY}{dx} = -\lambda x^{-2}\Delta(\Delta + 2Y_{EQ}), \tag{4.18}$$

substituting equation (4.18) into equation (4.15) yields

$$\frac{d\Delta}{dx} = -\frac{dY_{EQ}}{dx} - \lambda x^{-2}\Delta(\Delta + 2Y_{EQ}). \tag{4.19}$$

It is important to clarify that we begin by analyzing the system for $x > 1$ and $x \ll x_f$, where x_f represents the point of Freeze-out. Additionally, as mentioned earlier, Δ takes very small values and $\frac{d\Delta}{dx}$ also takes very small values. Therefore, we make the approximation $\frac{d\Delta}{dx} \approx 0$.

Taking this into account, we arrive at an approximate solution given by

$$\Delta \approx -\frac{x^2 Y'_{EQ}}{\lambda(\Delta + 2Y_{EQ})}, \tag{4.20}$$

Again, because Δ is very small compared to Y_{EQ}, it can be neglected in the denominator. Furthermore, we are working for $1 < x \ll x_f$, so the following consideration can be made using Equation (4.12):

$$\frac{Y'_{EQ}}{Y_{EQ}} = \frac{3}{2x} - 1 \approx -1. \tag{4.21}$$

Using these two approximations in Equation (4.20), we arrive at

$$\Delta \approx \frac{x^2}{2\lambda}. \tag{4.22}$$

Now we need to study the case after the Freeze-out to get a more complete understanding of how dark matter particles evolve during this transition. Consequently, we consider $x \gg x_f$. In this scenario, we can no longer treat Δ as a small quantity. A more appropriate approximation would be $\Delta \approx Y$, where $Y \gg Y_{EQ}$ because Y_{EQ} tends to zero for very high x values. Returning to Equation (4.20) with this in mind, and considering $Y_{EQ} \to 0$, we obtain

$$\Delta' \approx -\frac{\lambda}{x^2}\Delta^2, \tag{4.23}$$

this results in a differential equation that can be solved by separation of variables if expressed as

$$\frac{d\Delta}{\Delta^2} = -\frac{\lambda}{x^2}dx, \tag{4.24}$$

we then integrate both sides with respect to their respective variable to solve the equation

$$\int_{\Delta_f}^{\Delta_\infty} \Delta^{-2} d\Delta = -\lambda \int_{x_f}^{\infty} x^{-2} dx, \tag{4.25}$$

where the index ∞ represents the value of Y at present, and the index f its value at the time

of Freeze-out. Considering $Y_\infty \gg Y_f$ and additionally $Y_f = \Delta_f$, we can let the values of Y_f and Δ_f tend to zero, resulting in

$$Y_\infty = \Delta_\infty = \frac{x_f}{\lambda}. \tag{4.26}$$

It can be seen that the solution found represents the current number of dark matter relics in the universe per comoving volume. This is one of the equations that will be compared in the following sections.

4.2 Numerical process for the WIMP model

It is important to emphasize that there are no exact analytical solutions for the equation (4.10); however, an approximate solution can be obtained using numerical methods. In this section, numerical integration is used to achieve a result that agrees with what was found earlier through methods and analytical approximations. The first thing to consider is that, unlike in the analytical analysis, for the numerical case, it is necessary to know the values of all the constants that are going to be used and appear in our equation (4.10). To achieve this, we work with the form (4.16) and decompose λ, where $H(m)$ can be expressed as a function of $x = m/T$ a

$$H(m) = 1.66 g_*^{1/2} \frac{m^2}{x^2 m_{pl}}, \tag{4.27}$$

where m indicates the mass of the WIMP relic we are working with, for this project $m = 100$ GeV is used. It is also worth noting that the value of entropy s also changes as a function of x, following the expression

$$s = \frac{2\pi^2}{45} g_{*s} \frac{m^3}{x^3}. \tag{4.28}$$

With this data and equation (4.12), the complete form of the Boltzmann equation can be formulated to be solved numerically. To find this solution, the Python programming language and the numpy and scipy packages were used. The integrator used is a scipy method

called SolvIvp, which is used to solve ordinary differential equations. It is important to note that this method, like many other integrators available, defaults to the fourth-order Runge-Kutta method to find solutions. However, this presents a problem in this case because the differential equation undergoes abrupt changes in orders of magnitude. Consequently, it was necessary to try different methods.

It was concluded that the LSODA method works best for these problems because, unlike explicit methods like fourth-order Runge-Kutta, which compute solutions explicitly at each step, implicit methods like LSODA consider recurrence relationships between consecutive steps and can be more robust in situations where rates of change vary abruptly. This is because implicit methods allow the use of larger time steps without compromising stability and accuracy. What we want to find now is a curve for the thermodynamic evolution of the relics that agrees with the observed values of dark matter number density in the present $\Omega_c h^2 = 0.12 \pm 0.0012$ [5]. Remembering that the equation is in terms of Y, we make the following analysis to reach Y_0, which would be the observed value of Y at present [19], which has remained constant after freeze-out.

$$mY_0 = \Omega_{MO} h^2 \frac{1}{s_0} \frac{\rho_c}{h^2} = 4.3 \times 10^{-10} \pm 4.3 \times 10^{-12} \text{ GeV}, \tag{4.29}$$

with $\rho_c = 1.05 \times 10^{-5} h^2$ GeV/cm^3 being the critical energy density and $s_0 = 2.69 \times 10^3$ cm^{-3} the current entropy density. For now, the mass of the relics is considered as $m = 100$ GeV; later, the behavior of the solution will be observed when varying m, but for now, in this case, $Y_0 = 4.3 \times 10^{-12}$ GeV. Taking into account all the aforementioned factors, the solution was obtained as shown in Figure (4.2).

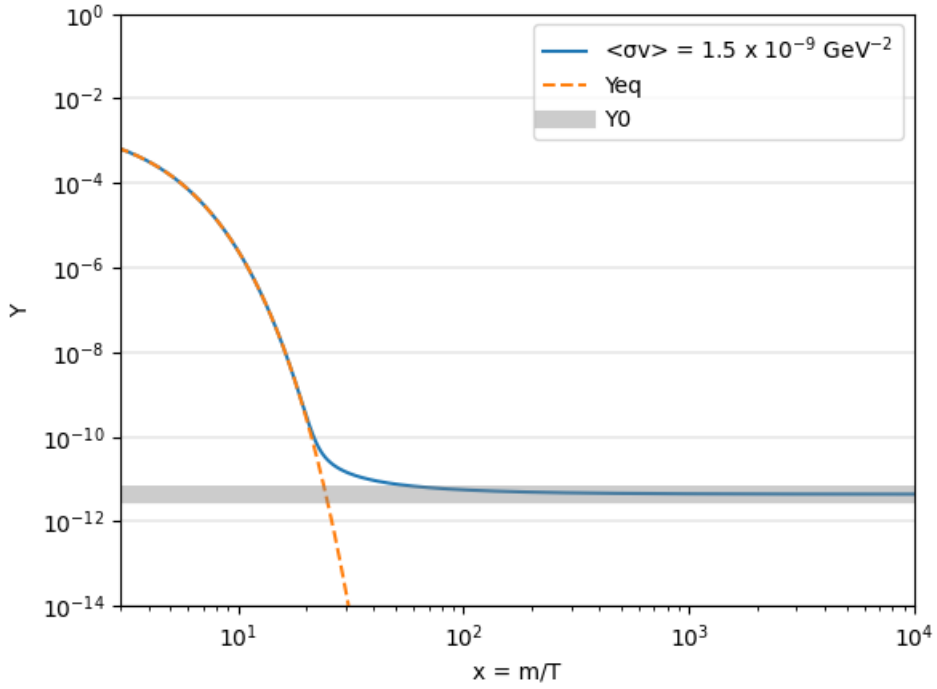

Figure 4.2: Numerical solution of equation (4.10) matching the estimated Y_0 for $m = 100$. The blue line represents the solution found with $\langle\sigma v\rangle = 1.5 \times 10^{-9}$ GeV^{-2}, the dashed orange line shows the evolution of the density in equilibrium, and the gray area indicates the approximate ranges of the current relic density values.

The figure (4.2) provides a lot of relevant information. Initially, it can be observed that the solution follows the equilibrium state, and when $x \approx 20$ is reached, the freeze-out begins because the interaction rate starts to decrease as discussed earlier, and the curve deviates from the equilibrium state until reaching the observed constant value. Additionally, it was found that the value of the cross-section that best fits the observed data is $\langle\sigma v\rangle = 1.5 \times 10^{-9}$ GeV^{-2}, and it can be seen in figure (4.3) how $\langle\sigma v\rangle$ is inversely proportional to the final Y after the freeze-out, which agrees with the theory, since a higher $\langle\sigma v\rangle$ leads to a higher interaction rate, causing fewer relics to survive before the freeze-out, resulting in a lower relic density.

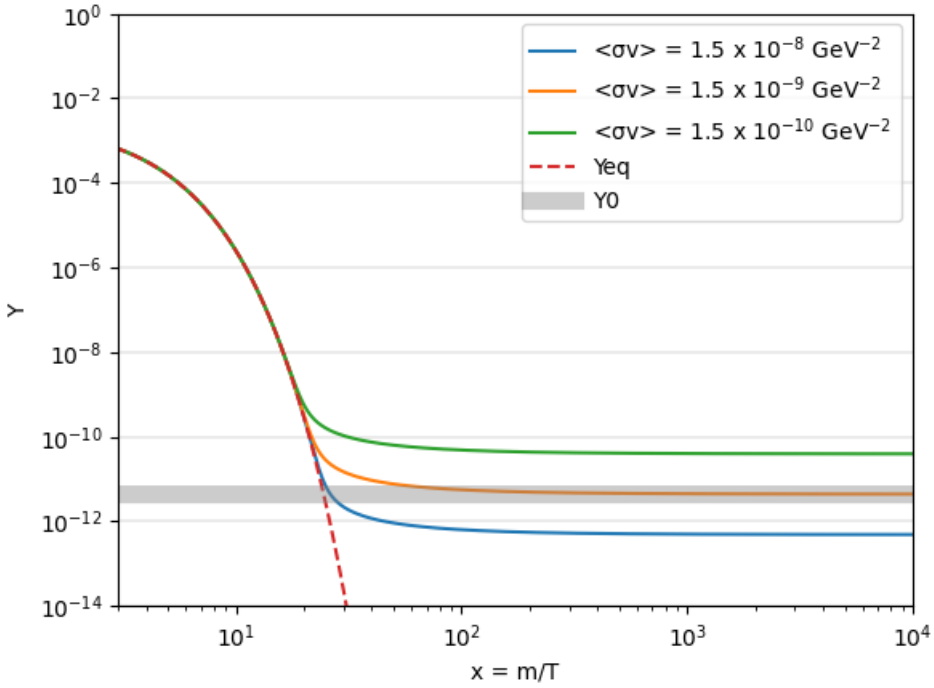

Figure 4.3: Numerical solution of equation (4.10) with $m = 100$ GeV for three possible corss sections, $\langle \sigma v \rangle = 1.5 \times 10^{-10} GeV^{-2}$ for the blue line, $\langle \sigma v \rangle = 1.5 \times 10^{-9} GeV^{-2}$ for the orange line and $\langle \sigma v \rangle = 1.5 \times 10^{-8} GeV^{-2}$ for the green line.

So far, solutions have been presented using a fixed mass of $m = 100$ GeV for the relics. Next, the analysis is conducted by varying the magnitude of m.

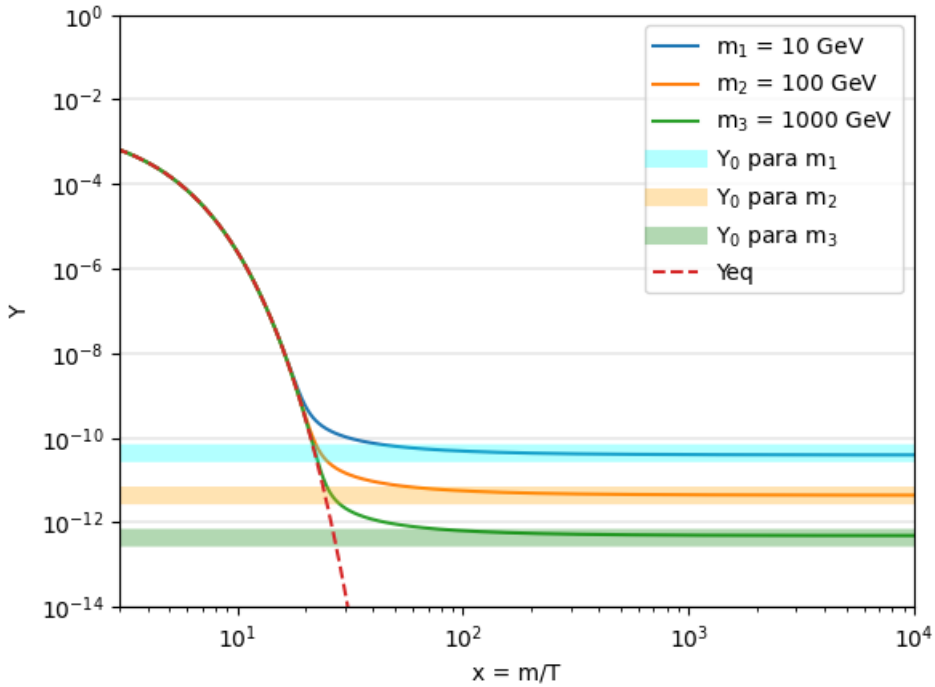

Figure 4.4: Effect of the mass of WIMP particles on the solution of equation (4.10) and on the observed Y_0. Here, for each value of m, its solution is shown with a solid line and its estimated Y_0. Blue represents $m = 10$ GeV, orange for $m = 100$ GeV, and green for $m = 1000$ GeV.

In Figure (4.4), it can be clearly seen that, like $\langle \sigma v \rangle$, the mass is also inversely proportional to Y, and according to equation (4.29), the observed density at present possesses the same relationship with m.

Finally, to clearly compare the analytically and numerically found solutions, they were plotted together for a value of $\langle \sigma v \rangle = 1.5 \times 10^{-9} GeV^{-2}$ and $m = 100$ GeV in Figure (4.5).

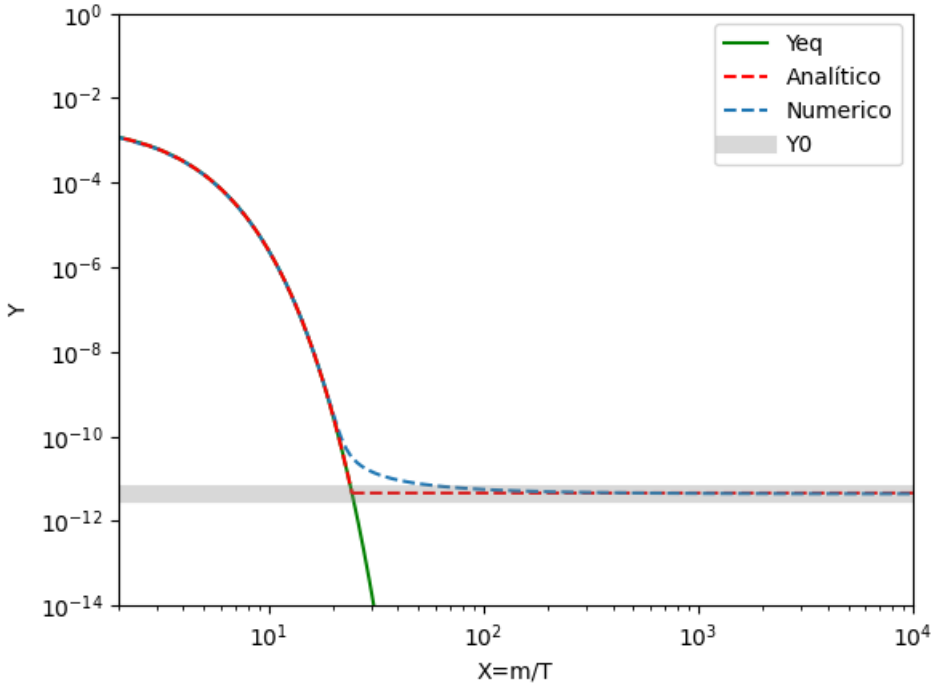

Figure 4.5: Analitical (blue line) and numerical solution (red line) of the equation (4.10) at $m = 100$ GeV.

It can be observed that the only moment where the solutions do not match is during the freeze-out. This is because the analytical result is a composite function where for $x < x_f$, it follows the equilibrium equation (4.12), and for $x > x_f$, it becomes the equation (4.26), which is a constant that depends on the freeze-out point x_f. Despite this, the solutions behave equivalently for high ranges of x, so both agree with the observed values [5].

4.3 Numerical process for the FIMP model

The numerical process used for the WIMP and FIMP mechanisms is very similar; the difference lies in the cross-section and the chosen initial values. The Boltzmann equation for WIMP can be used to find the solution for the FIMP mechanism, but the Y^2 term becomes negligible, so we can simplify the equation to the form

$$\frac{dY}{dx} = \lambda x^{-2} Y_{EQ}^2. \tag{4.30}$$

Something important to mention is that Equation (4.30) is no longer a stable differential equation like the one for WIMP, so the chosen initial values do affect the solution found. For this document, initial values of $x_0 = 10^{-1}$ and $y_0 = 0$ are used because the FIMP method involves a mechanism where it starts with a very low relic density and rapidly produces more until reaching the freeze-in point. In Figure (4.6), this behavior can be clearly seen. Unlike the WIMP mechanism, with this method, the relics do not follow the equilibrium curve, so they are not in thermal equilibrium, and likewise, the cross-section is directly proportional to the final relic density. This is an expected result because a higher $\langle \sigma v \rangle$ leads to a higher interaction rate, resulting in a higher relic density before reaching freeze-in.

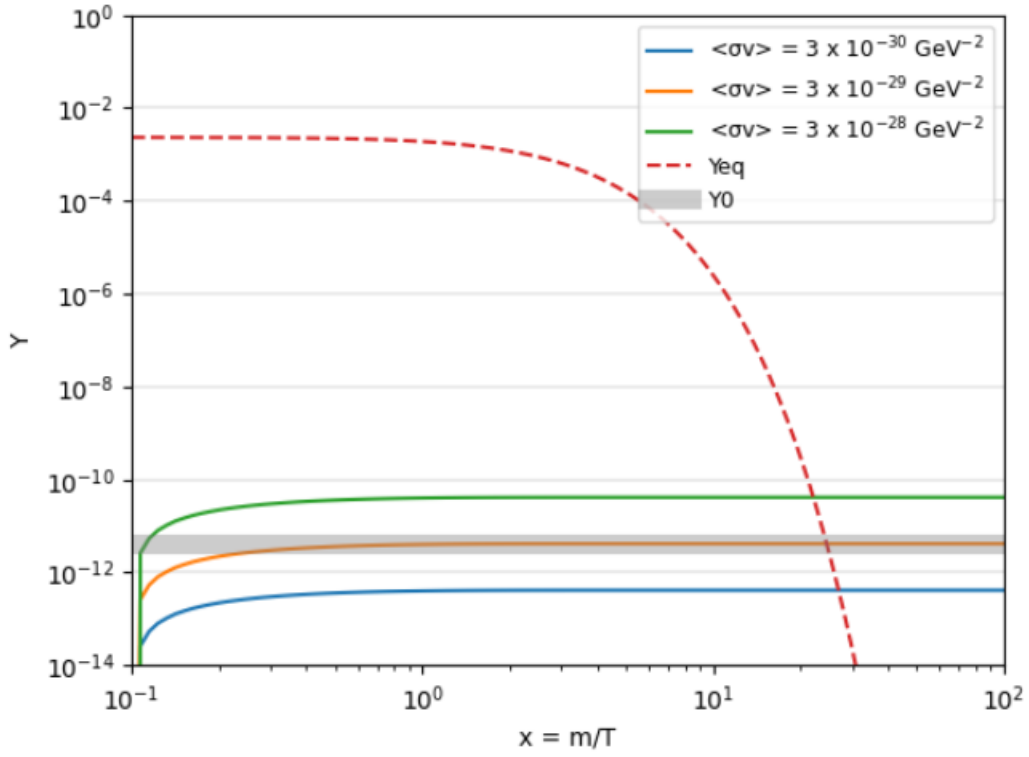

Figure 4.6: Numerical solution of the equation (4.30), which describes the FIMP mechanism at $m = 100$ GeV for three possible cross sections, $\langle \sigma v \rangle = 3 \times 10^{-30} GeV^{-2}$ for the blue line, $\langle \sigma v \rangle = 3 \times 10^{-29} GeV^{-2}$ for the orange line, and $\langle \sigma v \rangle = 3 \times 10^{-28} GeV^{-2}$ for the green line.

Additionally, it can be observed in Figure (4.6) how for $m = 100$ GeV and the initial values of $x_0 = 10^{-1}$ and $y_0 = 10^{-75}$, $\langle \sigma v \rangle = 1.5 \times 10^{-29}$ GeV^{-2} is needed to reach the observed relic density in the present universe. This value of $\langle \sigma v \rangle$ to achieve the desired density can vary

drastically when changing the other parameters of the system.

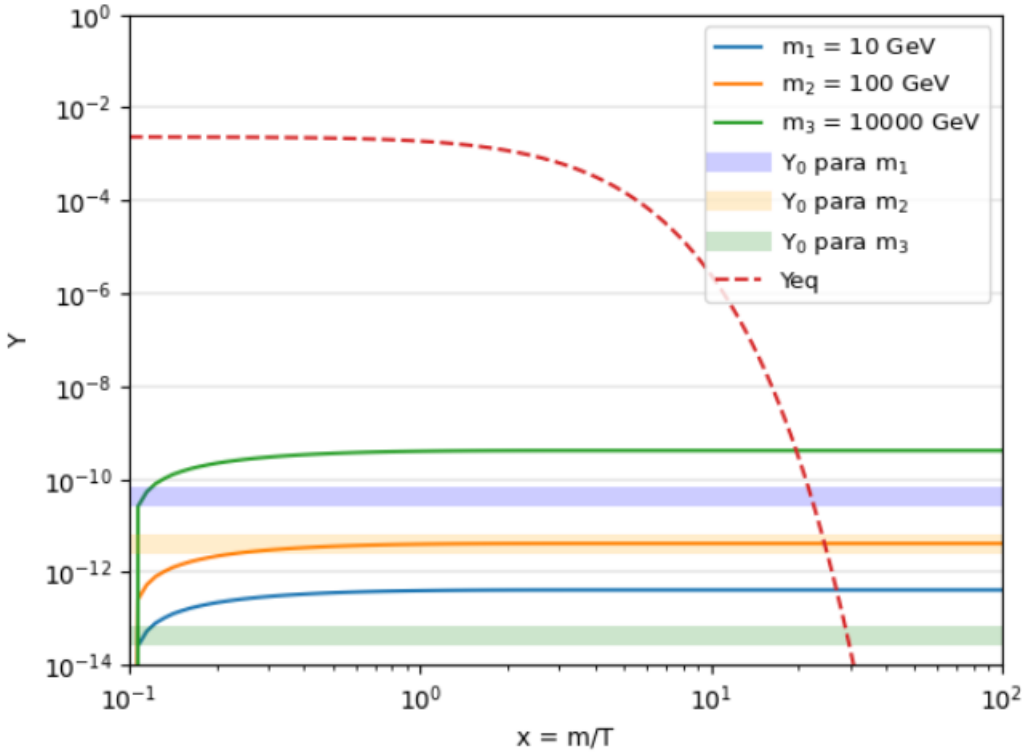

Figure 4.7: Effect of the mass of FIMP particles on the solution of equation (4.30) and on the observed Y_0 using $\langle \sigma v \rangle = 1.5 \times 10^{-29} GeV^{-2}$ and initial values of $x_0 = 10^{-1}$ and $y_0 = 10^{-75}$. For each value of m, its solution is represented by solid lines and its estimated Y_0 is indicated by horizontal bands, with blue color indicating $m = 10$ GeV, orange for $m = 100$ GeV, and green for $m = 10,000$ GeV.

The first observation from Figure (4.7) is how for masses $m = 10$ GeV and $m = 10,000$ GeV, their corresponding Y_0 values do not align with the obtained solutions. This is because m is directly proportional to the final solution, but Y_0 is inversely proportional as observed in equation (4.29). An attempt was made to find an approximate solution for the FIMP mechanism, but it turned out to be a much more complex task than expected, and it was not accomplished in this study.

4.4 Analitical process for the SIMP model

In this section, an analytical approximation of the SIMP mechanism is derived. To reach this approximation, similar methods to those used for the WIMP mechanism are employed. However, this time, we will use the Boltzmann differential equation for SIMP relics, equation (4.37). Remembering that we are finding an approximation for $x \to \infty$, we can consider $Y_{EQ} = 0$, which simplifies equation (4.37) to

$$\frac{dY}{dx} = -\frac{\langle \sigma v^2 \rangle \, s^2}{H(m)x} Y^3. \tag{4.31}$$

With this simplified form, the variable separable method can now be performed

$$\int_{x_f}^{\infty} Y^{-3} dY = -\int_{x_f}^{\infty} \frac{\langle \sigma |v|^2 \rangle \, s^2}{H(m)x} dx \tag{4.32}$$

$$-\frac{1}{2}(Y_{\infty}^{-2} - Y_{x_f}^{-2}) = -\int_{x_f}^{\infty} \frac{\langle \sigma |v|^2 \rangle \, s^2}{H(m)x} dx, \tag{4.33}$$

where we make the approximation $Y_{\infty} \ll Y_{x_f}$, resulting in

$$Y_{\infty}^{-2} = 2\int_{x_f}^{\infty} \frac{\langle \sigma |v|^2 \rangle \, s^2}{H(m)x} dx. \tag{4.34}$$

For these studies, the term $\langle \sigma |v|^2 \rangle$ has been considered constant, so we can take it out of the integral. Additionally, we replace s and $H(m)$ with equations (4.28) and (4.27) respectively:

$$\begin{aligned} Y_{\infty}^{-2} &= \frac{2 \langle \sigma |v|^2 \rangle \, (2\pi^2)^2 g_{*s}^2 m^6 m_{pl}}{(45)^2 (1,66) g_*^{1/2} m^2} \int_{x_f}^{\infty} \frac{x^2}{x^6 x} dx \\ &= \frac{(2)(2\pi^2)^2}{(45)^2(1,66)} \langle \sigma |v|^2 \rangle \, g_{*s}^2 m^4 m_{pl} g_*^{-1/2} (-\frac{1}{4})(x_{\infty}^{-4} - x_f^{-4}), \end{aligned} \tag{4.35}$$

Since $x_{\infty} \to \infty$, then $x_{\infty}^{-4} \approx 0$, giving the final result as:

$$Y_\infty = \left(\frac{2\pi^4}{(45)^2(1,66)} \langle \sigma |v|^2 \rangle \, g_{*s}^2 m^4 m_{pl} g_*^{-1/2} x_f^{-4}) \right)^{-1/2}, \tag{4.36}$$

The above expression can be graphed, comparing it to the result that will be found in the following section, which covers the numerical solution of the SIMP mechanism equation.

4.5 Numerical process for the SIMP model

Similar to the case of WIMP and FIMP, the first step in finding the solution will be to express our equation (3.23) in terms of $Y = n/s$ and $x = m/T$. Making these variable changes, the differential equation for the SIMP mechanism would be represented as:

$$\frac{dY}{dx} = -\frac{\langle \sigma v^2 \rangle \, s^2}{H(m)x}(Y^3 - Y^2 Y_{EQ}), \tag{4.37}$$

The differential equation describing the evolution of SIMP relics, like the equations studied previously, does not have an exact analytical solution. Therefore, we will initiate the study by finding the numerical solution using methods very similar to those used for the other two mechanisms. As mentioned for the cases of WIMP and FIMP, these equations are known as stiff differential equations, which undergo abrupt magnitude changes at each step in the numerical solution. For the SIMP mechanism, this phenomenon is even stronger, so the solution found begins closer to the freeze-out point to process the transition more smoothly.

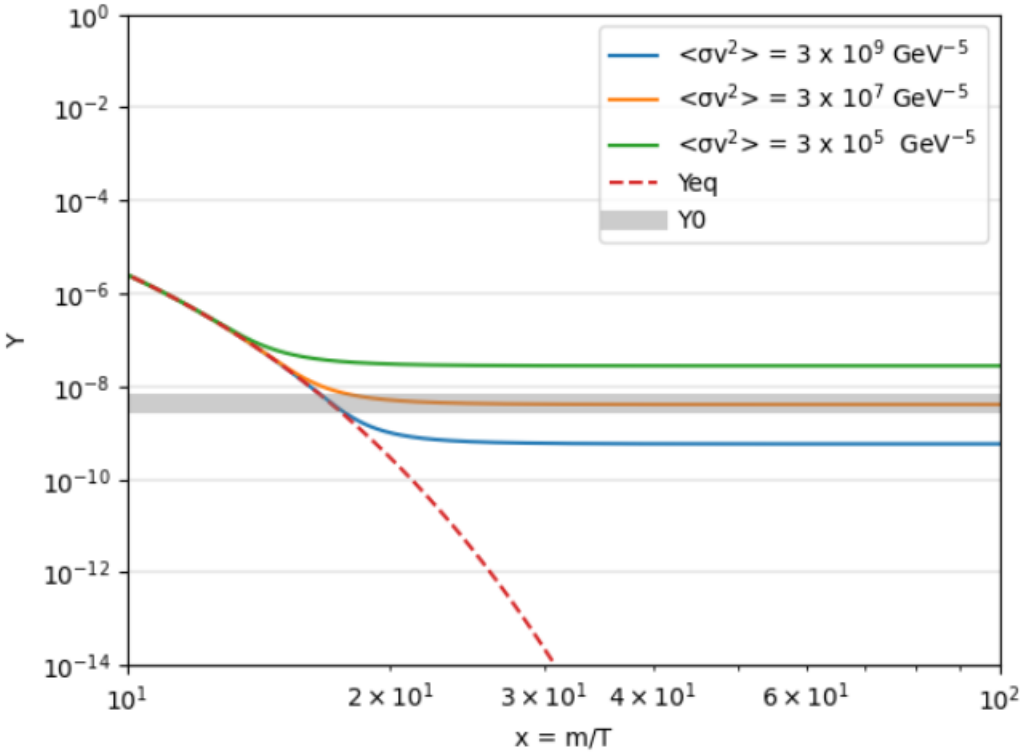

Figure 4.8: Effect of varying the parameter $\langle \sigma v^2 \rangle$ on the solution of the differential equation for the SIMP mechanism (4.37) for a mass of 100 MeV. The blue line corresponds to $\langle \sigma v^2 \rangle = 3 \times 10^9 \text{GeV}^{-5}$, the orange line to $\langle \sigma v^2 \rangle = 3 \times 10^7 \text{GeV}^{-5}$, and the green line to $\langle \sigma v^2 \rangle = 3 \times 10^9 \text{ GeV}^{-5}$. The estimated Y_0 for $m = 100$ GeV is shown in the horizontal gray band.

At first glance, the behavior of Y in Figure (4.8) can be observed to be very similar to what was found for the WIMP mechanism. The term $\langle \sigma v^2 \rangle$ is again inversely proportional to the final number density after freeze-out. In previous systems, this term was referred to as the cross section, but now, due to the velocity being squared, it cannot be referred to in this way. Additionally, since the collision involves three particles simultaneously, the concept of cross section for this mechanism becomes somewhat more symbolic. Therefore, the term $\langle \sigma v^2 \rangle$ takes larger values than expected, as seen in Figure (4.8), where for a mass of 100 GeV, it is necessary to use $\langle \sigma v^2 \rangle = 3 \times 10^2 \text{ GeV}^{-5}$ to reach the observed values of the current number density. An important detail is that for the SIMP mechanism, we are no longer working with masses in the GeV range but rather in the MeV range. This is because demanding perturbative couplings for interaction, the SIMP mass typically tends to values

below a GeV. Another significant difference between the WIMP and SIMP mechanisms is how, after freeze-out, the SIMP system reaches its Y_0 value faster than in the case of WIMP relics.

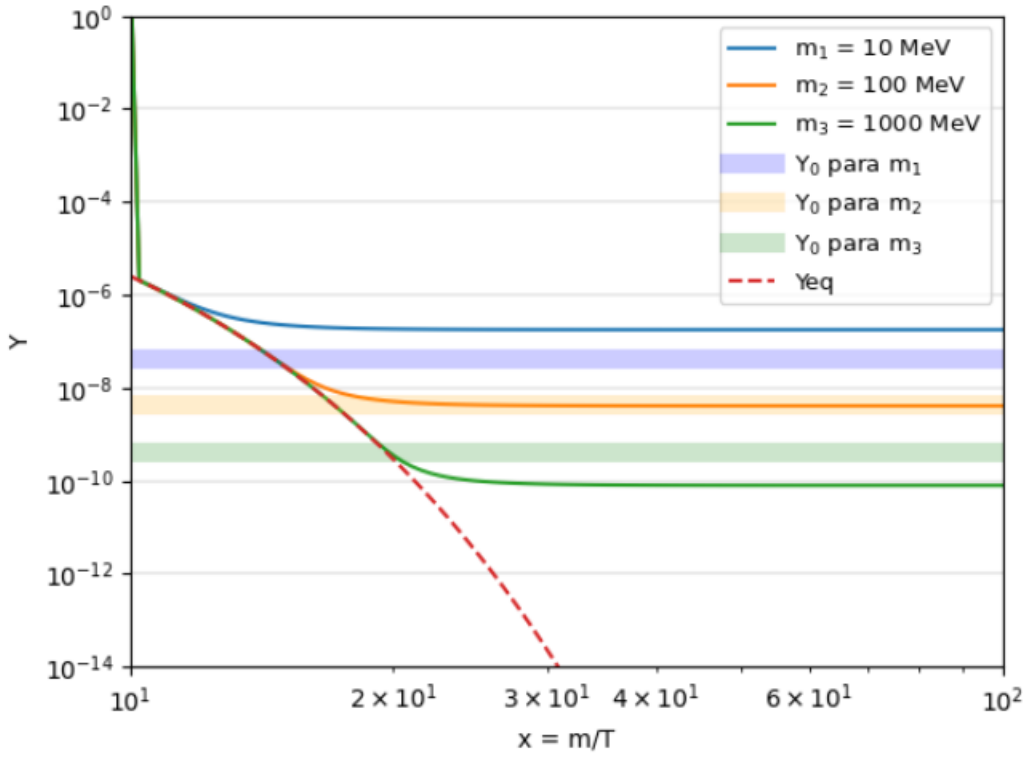

Figure 4.9: Effect of varying the mass of SIMP relics on the solution of the differential equation for the SIMP mechanism (4.37) for $\langle \sigma v^2 \rangle = 3 \times 10^2$ GeV^{-5}. The blue line corresponds to $m = 10$MeV, the orange line to $m = 100$MeV, and the green line to $m = 1000$ MeV. The estimated Y_0 for each mass is shown in the horizontal stripes corresponding to the respective colored lines.

In the figure (4.9), different behaviors from the previously studied cases can be observed, where the mass is inversely proportional to the final density, but it does not vary in the same way as the term $\langle \sigma v^2 \rangle$. As seen, when increasing or decreasing the mass of the relics, the final Y is different from the Y_0 predicted by observations. To make these two results agree, the term $\langle \sigma v^2 \rangle$ needs to be varied so that for $m = 10$ MeV, $\langle \sigma v^2 \rangle = 10^9$ GeV^{-5} is used, and for $m = 1000$ MeV, it would be $\langle \sigma v^2 \rangle = 10^6$ GeV^{-5}. Another very interesting phenomenon that can be observed in figure (4.9) is that for $x = 10$, there is a significant drop in the green line, which is superimposed with the blue and orange lines. This shows how the SIMP differential

equation (4.37), like the WIMP equation (4.9), are stable differential equations, which are not affected by the initial value used, as they will always reach the same point as soon as the solution starts. This behavior could be observed in the other WIMP and SIMP graphs if initial parameter values were used further away from the starting point of Y_{EQ}.

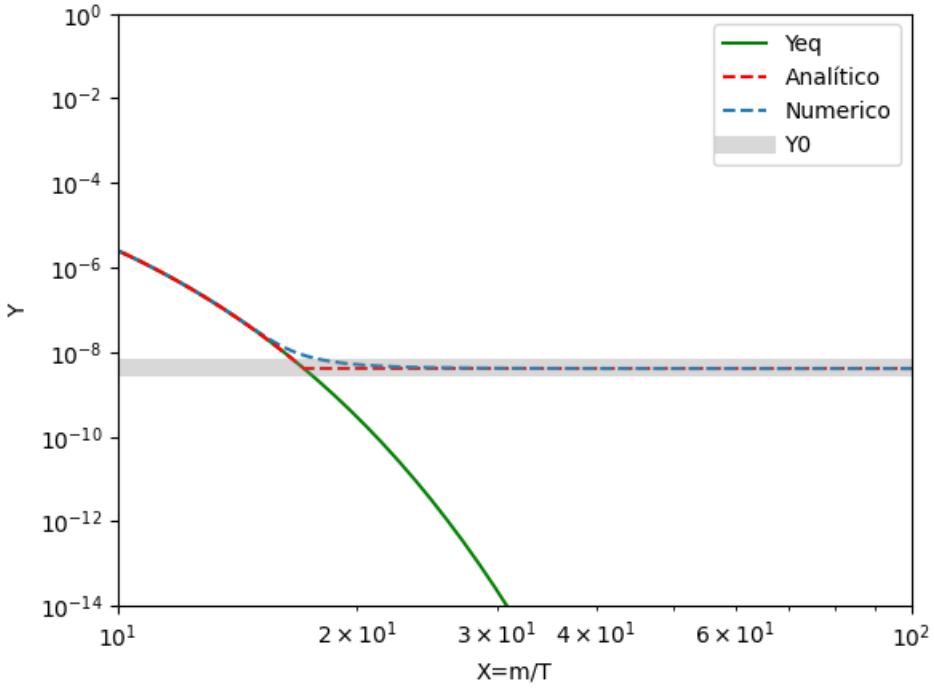

Figure 4.10: In the figure (**??**), the analytical and numerical solutions of the SIMP mechanism for $m = 100$ MeV and $\langle \sigma v^2 \rangle = 3 \times 10^2$ GeV^{-2} are compared.

In the figure (**??**), the comparison between the analytical solution and the numerical solution found for equation (4.37) can be observed. Similar to the WIMP mechanism case, the approximate analytical solution is a composite function, where for $x < x_f$ the equation (4.11) is followed, and then after x_f, the solution found previously in equation (**??**) is used. This approximation is even more accurate than for the WIMP method because the transition from following equilibrium to freeze-out occurs very quickly for the SIMP mechanism.

4.6 Final results

It can be observed that there are clear differences in the thermodynamic evolution of each studied mechanism despite many conceptual similarities. To better appreciate the behavior of WIMP, FIMP, and SIMP relics, their solutions are plotted on the same diagram.

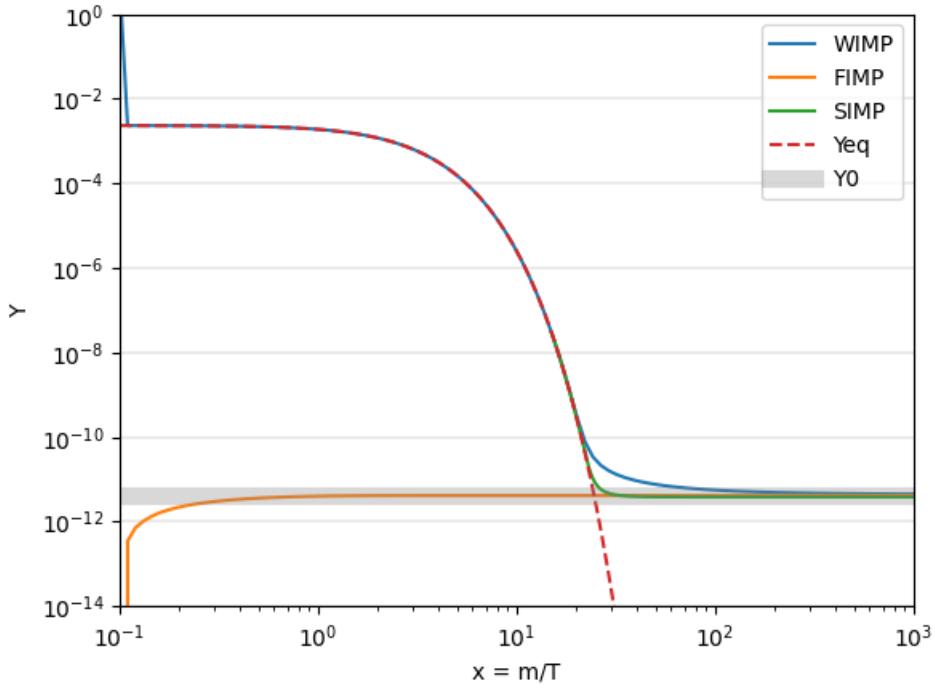

Figure 4.11: Evolution of the density of WIMP, FIMP, and SIMP relics considering a mass of 100 GeV.

In the figure (4.11), a final comparison of the three analyses is presented. Initially, a sharp drop can be observed for the WIMP mechanism at very early times, which is the same phenomenon mentioned for SIMP relics, but not evident for SIMP because its initial values were set at its starting point at $x = 15$. Additionally, the difference in time taken for the WIMP mechanism to reach its final value compared to SIMP is more evident. This is because it is more difficult for the SIMP interaction to occur once it goes out of thermal equilibrium due to the $3 \rightarrow 2$ nature of annihilation. On the other hand, the FIMP mechanism never follows Y_{EQ} and is highly dependent on its initial values $y_0 = 10^{-75}$ and $x_0 = 10^{-1}$, evidenced by its freeze-in point, which is practically at x_0.

Chapter 5

Conclusiones

In this study, significant differences were observed among the mechanisms of WIMP, FIMP, and SIMP dark matter production. Specific analytical and numerical methods were employed to perform the necessary calculations. The LSODA method and the solve-ivp function from the Scipy package in Python were used. Careful calibration of solution tolerance parameters and resolution step size was essential to obtain accurate results and properly observe the generated graphs in the study.

For the WIMP and SIMP mechanisms, in addition to numerical calculations, an approximate solution was found that closely matched the results obtained using numerical methods, indicating the existence of an effective analytical approach for these mechanisms. In both the WIMP and SIMP mechanisms, it was found that particles followed thermal equilibrium for most of the dark matter production process, meaning that the density of dark matter particles remained in equilibrium with standard model particles until freeze-out occurred.

One interesting finding was that the SIMP mechanism transitioned more rapidly from its freeze-out point to its final constant value compared to the WIMP mechanism, suggesting a more efficient interaction in transitioning to its non-relativistic state. On the other hand, the FIMP mechanism stood out for not following thermal equilibrium at any point, and it was

noted to be highly sensitive to the initial conditions used in the calculations. This underscores the critical importance of initial conditions in dark matter production via the FIMP mechanism and the need for careful consideration in analyses.

It was also found that in the WIMP and SIMP mechanisms, there was an inversely proportional relationship between the relic mass and the effective cross-section used with the final number density of dark matter particles, where $Y \propto \frac{1}{m\langle\sigma v\rangle}$ for WIMP and $Y \propto \frac{1}{m^2\sqrt{\langle\sigma v^2\rangle}}$ for SIMP. On the other hand, in the case of the FIMP mechanism, a directly proportional relationship was found between the relic mass and the effective cross-section used with the final number density of dark matter particles, of the form $Y \propto m\,\langle\sigma v\rangle$.

Additionally, each of the studied cases was compared with relevant observational data, and it was found that the results obtained were consistent with observed data when appropriate values of cross-section and relic mass were used. This supports the validity of the models and approaches used in this research. This document provided a deeper review of dark matter production in the primordial universe through different mechanisms. The key differences between WIMP, FIMP, and SIMP mechanisms were highlighted, as well as the importance of numerical methods and initial conditions in the results obtained. These findings also contribute to the advancement of knowledge in the field of particle physics and high-energy physics and have important implications for understanding dark matter in the early universe, supported by the congruence of the results with observational data.

The future of research on these production mechanisms has great potential despite the elusive nature of these particles, making their detection a major challenge. For WIMP mechanisms, attempts have been made to test them using a variety of experiments, both direct detection and indirect detection. Examples include experiments conducted by the LUX-ZEPELIN or XENON10 detectors for direct detection and analyses of observations made by the Fermi-LAT, looking for gamma-ray signals that may be caused by WIMP annihilation in regions of high dark matter concentration.

For FIMP particles, they are characterized by their very weak interaction with standard matter, making them very difficult to detect through collision experiments, such as those conducted at the Large Hadron Collider or even fixed-target experiments. Fortunately, new direct detection techniques for particles with lower energy ranges, such as some FIMP candidates, especially sterile neutrinos, have begun to be developed. One advantage that these light candidates may have is that to reach the current abundance of dark matter, they would need to have a higher number density than other candidates, thus increasing the detection rate. These new experimental techniques focus on dark matter in the keV to MeV ranges.

On the other hand, for SIMP particles, indirect detection experiments are very useful. This is because SIMPs interact heavily with each other, and these interactions could release very energetic gamma-ray signals, which are possible to detect and study. The detection and observation of these gamma-ray signals are one of the main focuses of the Fermi-LAT telescope. This makes it clear that many, though not all, experiments conducted to test WIMP particles can be used to study the possible existence of FIMPs and SIMPs.

Appendix A

Boltzmann equation for the WIMP mechanism

In this section, we will analyze in detail how we arrived at the equation (3.22). We begin by setting up the evolution of the distribution function of species χ entering or leaving equilibrium using the Boltzmann equation.

$$\hat{L}[f_\chi] = \hat{C}[f_\chi], \tag{A.1}$$

where $\hat{L}$ is the Liouville operator and parameterizes the changes in phase-space density over time, $\hat{C}$ is the collision operator and parameterizes the number of particles per phase-space volume, and f_χ is the phase-space density of species χ.

With this established, we begin the development for the Liouville operator, which in Friedmann–Lemaître–Robertson–Walker cosmology, where $f = (E, t)$ is considered, becomes:

$$\hat{L}\,[f_\chi] = \frac{df_\chi}{dt} = \frac{\partial f_\chi}{\partial t} + \frac{\partial f_\chi}{\partial E}\frac{dE}{dt}, \tag{A.2}$$

Where $E = \sqrt{\vec{p}^2 + \vec{m}^2}$, and if we keep searching for the derative

$$\frac{dE}{dt} = \frac{1}{2\sqrt{\vec{p}^2 + m^2}} 2\vec{p} \cdot \frac{d\vec{p}}{dt} = \frac{\vec{p}}{E} \cdot \frac{d\vec{p}}{dt} = \frac{\vec{p}}{E} \cdot \frac{d\vec{p}}{da}\frac{da}{dt} = -\frac{p^2}{E}H, \tag{A.3}$$

Now, considering that $\vec{p}$ is a function of the scale factor a, and that the non-relativistic momentum is $p \propto a^{-1}$, this implies that $\frac{d\vec{p}}{da} = -\frac{\vec{p}}{a}$, which leads to

$$\frac{dE}{dt} = \frac{\vec{p}}{E} \cdot \frac{d\vec{p}}{da}\frac{da}{dt} = -\frac{\vec{p}}{E} \cdot \frac{\dot{a}\vec{p}}{a}, \tag{A.4}$$

remembering that $H = \frac{\dot{a}}{a}$ we get

$$\frac{dE}{dt} = -\frac{p^2}{E}H, \tag{A.5}$$

Replacing this in the Liouville operator we get

$$\hat{L}\left[f_\chi\right] = \frac{df_\chi}{dt} = \frac{\partial f_\chi}{\partial t} - \frac{\partial f_\chi}{\partial E}\frac{p^2}{E}H. \tag{A.6}$$

The goal is to rewrite this operator in terms of the number density of χ particles, which is defined as

$$n_\chi(T) = \frac{g}{(2\pi)^3}\int f_\chi(E,T)d^3\vec{p}, \tag{A.7}$$

using the substitution method $d^3\vec{p} = 4\pi|\vec{p}|^2 d|\vec{p}| = 4\pi|\vec{p}|EdE$

$$n_\chi(T) = \frac{g}{2\pi^2}\int_m^\infty f_\chi(E,T)\sqrt{E^2 - m^2}EdE, \tag{A.8}$$

To make the Liouville operator take a form similar to equation (**??**), we multiply it by $\frac{g}{(2\pi)^3}$ and integrate it with respect to $d^3\vec{p}$,

$$\begin{aligned}\frac{g}{(2\pi)^3}\int \hat{L}\left[f_\chi\right]d^3\vec{p} &= \frac{g}{2\pi^2}\int_m^\infty \left[\frac{\partial f_\chi}{\partial t} - \frac{\partial f_\chi}{\partial E}\frac{p^2}{E}H\right]\sqrt{E^2 - m^2}EdE \\ &= \frac{g}{2\pi^2}\int_m^\infty \frac{\partial f_\chi}{\partial t}\sqrt{E^2 - m^2}EdE - \frac{gH}{2\pi^2}\int_m^\infty \frac{\partial f_\chi}{\partial E}\left(E^2 - m^2\right)^{3/2}dE,\end{aligned} \tag{A.9}$$

You can notice that the first integral is $\frac{n_\chi}{dt}$ and the second one can be solved using integration by parts, taking $u = \left(E^2 - m^2\right)^{3/2}$ and $dv = \frac{\partial f_\chi}{\partial E}dE$. This leads to

$$\begin{aligned}\frac{g}{(2\pi)^3}\int \hat{L}\left[f_\chi\right] d^3\vec{p} &= \frac{dn_\chi}{dt} - \frac{gH}{2\pi^2}\left[\cancel{\left(E^2-m^2\right)^{3/2} f_\chi\Big|_m^\infty} - 3\int_m^\infty E\sqrt{E^2-m^2} f_\chi dE\right] \\ &= \frac{dn_\chi}{dt} + 3Hn_\chi.\end{aligned} \tag{A.10}$$

Having the Liouville operator written in this form, we can reexpress the Boltzmann equation as

$$\frac{dn_\chi}{dt} + 3Hn = \frac{g}{(2\pi)^3}\int \frac{C[f]}{E} d^3p. \tag{A.11}$$

This equation is valid for different types of interactions depending on the collision operator used. For this case, we initially consider a process $X \to Y$, where the collision operator for a particle k is defined as [16]

$$\begin{aligned}&\frac{g}{(2\pi)^3}\int \hat{C}\left[f_\chi\right] d^3\vec{p} \\ &= \sum_{X,Y} r_k \int \frac{d\Pi_X}{S_X}\frac{d\Pi_Y}{S_Y}(2\pi)^4\delta^{(4)}\left(p_X - p_Y\right)\left(\prod_{i\in X} f_i\right)\left(\prod_{j\in Y}\left(1 \pm f_j\right)\right)\left|\mathcal{M}(X\to Y)\right|^2,\end{aligned} \tag{A.12}$$

This is a compressed form of Equation (3.15), where the summation covers all processes involving particle k, which can be part of multi-particle states X and Y. Here, $r_k = \bar{n}_k(-\bar{n}_k)$, where k in $Y(X)$ counts the $\bar{n}_k > 0$ of particles k in $Y(X)$. Π_X and Π_Y are the Lorentz invariant spatial phase integration factors.

$$d\Pi_X = \prod_{i\in X}\frac{d^4p_i}{(2\pi)^4} 2\pi\delta\left(p_i^2 - m_i^2\right)\theta\left(p_i^0\right) = \prod_{i\in X}\frac{d^3p_i}{(2\pi)^3 2E_i}, \tag{A.13}$$

$$d\Pi_Y = \prod_{i\in Y}\frac{d^3p_i}{(2\pi)^3 2E_i}, \tag{A.14}$$

$S_X(S_Y)$ is the symmetry factor that counts the identical particles in $X(Y)$, $p_X = \sum_{i\in X} P_i$ and $p_Y = \sum_{i\in Y} P_i$ are the sum of the four-momenta in $X(Y)$, f_i are the distribution functions. Finally, $|M(X\to Y)|^2$ is the matrix of elements for the interaction $X \to Y$. To simplify the

collision operator, we make three approximations. The first is that we do not consider the Pauli exclusion principle or Bose enhancement, making

$$(1 \pm f_j) \to 1. \tag{A.15}$$

For the second approximation, we consider that the interacting particles are in kinetic equilibrium at a temperature T, so that their out-of-equilibrium distribution function is proportionate to their distribution function when they are in equilibrium.

$$f_i = f_i^{eq}(T)\frac{n_i}{n_i^{eq}(T)}. \tag{A.16}$$

For the third approximation, we assume that the Maxwell-Boltzmann statistics are followed for the equilibrium distributions.

$$\Pi_{i\in X} f_i^{eq} = e^{-\frac{E_X}{T}}, \tag{A.17}$$

where $E_X = \sum_{i\in X} E_i$. With these approximations, the collision operator can be simplified to

$$\frac{g}{(2\pi)^3}\int \hat{C}\left[f_\chi\right] d^3\vec{p} = \sum_{x\to Y} \mathcal{N}(k, X \to Y) \times \gamma(X \to Y), \tag{A.18}$$

where the shift factor, which quantifies the departure from chemical equilibrium, is defined as

$$\mathcal{N}(k, X \to Y) = r_k \prod_{i\in X} \frac{n_i}{n_i^2}, \tag{A.19}$$

and the collision rate density, which quantifies the number of interactions per unit time and volume, is defined as

$$\gamma(X \to Y) \equiv \int \frac{d\Pi_X}{S_X}\int \frac{d\Pi_Y}{S_Y}(2\pi)^4\delta^{(4)}\left(p_X - p_Y\right) e^{-\frac{E_X}{T}} |\mathcal{M}(X \to Y)|^2. \tag{A.20}$$

With this, we arrive at a simplified form of the collision operator that can be used for a

variety of particle interactions. To make it specific for the case of the WIMP mechanism, which involves a $2 \rightarrow 2$ interaction and experiences a freeze-out point, we need to make certain considerations to solve the collision operator. First, it's important to remember that we are dealing with dark matter particles, which are considered stable or with a lifetime greater than the age of the universe. The most relevant reactions are then given by

$$\begin{aligned} X + X &\longleftrightarrow i + j, \\ X + \bar{X} &\longleftrightarrow i + j, \end{aligned} \tag{A.21}$$

Where i and j are standard model particles and $2m_X > m_i + m_j$. Higher-order interactions ($2 \leftrightarrow 3$, $3 \leftrightarrow 3$, etc.) are not considered as they are typically very minor. Another consideration is that if the dark matter particle is its own antiparticle, then $X + X \leftrightarrow e^+e^-$ implies $2\mu_X = \mu_{e^+} + \mu_{e^-} = 0$. If it is not its own antiparticle but there is no asymmetry between dark matter and anti-dark matter, then $\mu_X = \mu_{\bar{X}} = 0$. It is also important to remember that i and j are in equilibrium, so $f_i = f_i^{eq}$. Finally, energy conservation $E_X + E_{\bar{X}} = E_i + E_j$ leads to $f_i f_i^{eq} = f_X f_{\bar{X}}$.

With all these considerations, the collision operator can be written as

$$\frac{g}{(2\pi)^3} \int \hat{C}\left[f_\chi\right] d^3\vec{p} = -\left\langle \sigma v \right\rangle \left[n_X^2 - (n_X^{eq})^2\right], \tag{A.22}$$

Where $\langle \sigma v \rangle$ is the cross section multiplied by the relative velocity, containing

$$\langle \sigma v \rangle = \frac{1}{(n_\chi^{\mathrm{eq}})^2} \int d\Pi_\chi d\Pi_{\bar{\chi}} d\Pi_i d\Pi_j (2\pi)^4 \delta^4 \left(p_\chi + p_{\bar{\chi}} - p_i - p_j\right) |\mathcal{M}|^2 e^{-\frac{E_\chi + E_{\bar{\chi}}}{T}}. \tag{A.23}$$

Replacing the Liouville operator and the collision operator found in the initial Boltzmann equation, we conclude

$$\dot{n}_\chi + 3Hn_\chi = -\langle \sigma v \rangle \left[n_\chi^2 - \left(n_\chi^{\mathrm{eq}}\right)^2\right]. \tag{A.24}$$

This is the Boltzmann equation that was worked on for the WIMP production mechanism.

Bibliography

[1] A. Arbey and F. Mahmoudi. Dark matter and the early universe: A review. *Progress in Particle and Nuclear Physics*, Abril 2021.

[2] Fritz Zwicky. Luminous and dark formations of intergalactic matter. *Physics Today*, 1953.

[3] Anatolii Vladimirovich Zasov, Ann S Saburova, Alexander Valentinovich Khoperskov, and Sergey A Khoperskov. Dark matter in galaxies. *Physics-Uspekhi*, page 3, 2017.

[4] Albert Bosma. Rotation curves and the dark matter problem. *arXiv preprint arXiv:2309.06390*, 2023.

[5] Nabila Aghanim, Yashar Akrami, Mark Ashdown, J Aumont, C Baccigalupi, M Ballardini, AJ Banday, RB Barreiro, N Bartolo, S Basak, et al. Planck 2018 results-vi. cosmological parameters. *Astronomy & Astrophysics*, 2020.

[6] N Mandolesi and Fabrizio Villa. First/planck mission. In *IMTC/99. Proceedings of the 16th IEEE Instrumentation and Measurement Technology Conference (Cat. No. 99CH36309)*, volume 2, pages 975–980. IEEE, 1999.

[7] Stefano Profumo. *An introduction to particle dark matter*. World Scientific Publishing Company, 2017.

[8] Stefano Profumo, Leonardo Giani, and Oliver F Piattella. An introduction to particle dark matter. *Universe*, 2019.

[9] Nathaniel Craig and Andrey Katz. The fraternal wimp miracle. *Journal of Cosmology and Astroparticle Physics*, 2015(10):054, 2015.

[10] Stefano Giagu. Wimp dark matter searches with the atlas detector at the lhc. *Frontiers in Physics*, 2019.

[11] Jodi Cooley. Dark matter direct detection of classical wimps. *arXiv preprint*, 2021.

[12] Jelle Aalbers, DS Akerib, CW Akerlof, AK Al Musalhi, F Alder, A Alqahtani, SK Alsum, CS Amarasinghe, A Ames, TJ Anderson, et al. First dark matter search results from the lux-zeplin (lz) experiment. *arXiv preprint arXiv:2207.03764*, 2022.

[13] J Ballet, P Bruel, TH Burnett, B Lott, et al. Fermi large area telescope fourth source catalog data release 4 (4fgl-dr4). *arXiv preprint arXiv:2307.12546*, 2023.

[14] Edward W Kolb and Michael S Turner. *The early universe*. CRC press, 2018.

[15] Lawrence J Hall, Karsten Jedamzik, John March-Russell, and Stephen M West. Freeze-in production of fimp dark matter. *Journal of High Energy Physics*, 2010.

[16] Nicolás Bernal, Matti Heikinheimo, Tommi Tenkanen, Kimmo Tuominen, and Ville Vaskonen. The dawn of fimp dark matter: a review of models and constraints. *International Journal of Modern Physics A*, 2017.

[17] Yonit Hochberg, Eric Kuflik, Tomer Volansky, and Jay G. Wacker. Mechanism for thermal relic dark matter of strongly interacting massive particles. *Physical Review Letters*, oct 2014.

[18] Lin Fei. *Dark matter dynamics in the early universe*. PhD thesis, Massachusetts Institute of Technology, 2012.

[19] Nicolás Bernal and Yong Xu. Wimps during reheating. *Journal of Cosmology and Astroparticle Physics*, 2022(12):017, 2022.